time) is in operation on the CDC 7600.[3] A three-dimensional calculation with the same detail as the two-dimensional calculation presented here would require 35 times the number of zones and four quadrants instead of one. The total number of zones required would be 140 times the number used and the computer time would increase by the same factor. By replacing the IBM 7030 with the STAR computer, a 150 fold increase in computation speed is achieved. This more than offsets the increase in computation time required for a similar three-dimensional calculation. Thus, with the STAR computer, it will be possible to simulate the general three-dimensional problem of a body moving through air at a finite angle of attack in the same computer time as the two dimensional problem given here.

References

[1] Von Neumann, J. and Richtmyer, R. D., "A Method for the Numerical Calculation of Hydrodynamic Shocks," *Journal of Applied Physics*, Vol. 21, No. 3, March 1950, pp. 232–237.

[2] Wilkins, M. L., "Calculation of Elastic Plastic Flow," UCRL-7322 Rev. I, Jan. 24, 1969, Lawrence Radiation Lab., Livermore, Calif.

[3] Wilkins, M. L., French, S. J., and Sorem, M., "Finite Difference Scheme for Calculating Problems in Three Space Dimensions and Time," UCRL-72634, Aug. 13, 1970, Lawrence Radiation Lab., Livermore, Calif.

Exact Numerical Solutions for Transient Shear Stress and Boundary-Layer Induced Pressure

Czeslaw M. Rodkiewicz*
University of Alberta, Edmonton, Canada

AND

Roop N. Gupta†
NASA Langley Research Center, Hampton, Va.

Nomenclature

C = $\mu\rho/\mu_\infty\rho_\infty$
f = function related to the stream function by $\psi = [2\nu_\infty CtU_\infty]^{1/2} f(\eta,\xi)$
Δf = $f - f_2$
h = local enthalpy
H = total enthalpy, $= h + u^2/2$
I = $\int_0^\infty \left\{ S_w + \frac{[(\gamma-1)/2]M_\infty^2}{(1+[(\gamma-1)/2]M_\infty^2)} f' \right\} (1-f')d\eta$
J = $\int_0^\infty [1-f']d\eta$
M_∞ = freestream Mach number
Pr = Prandtl number
p = Static pressure
Δp = $p_{w,2} - p_w$
Re_{x_∞} = $\rho_\infty U_\infty x/\mu_\infty$
S = total enthalpy ratio, $= H/H_\infty$
t = time
u = x-component of velocity
U = plate velocity
ΔU = impulsive change in plate velocity, $= (U_2 - U_1)_\infty$
x,y = coordinates along and normal to the plate, respectively
γ = ratio of specific heats
δ_ρ = density defect thickness, $\int_0^\infty \left(1 - \frac{\rho}{\rho_\infty}\right) dy$
δ^* = mass flow defect thickness, $\int_0^\infty \left[1 - \frac{\rho u}{(\rho U)_\infty}\right] dy$
ξ = similarity independent variable associated with time and space, $= (U_\infty t/x)/(U_\infty t/x) + 1$
η = similarity independent variable associated with space, $= \left[\frac{U_\infty}{2\nu_\infty Cx}\right]^{1/2} \int_0^y \frac{\rho}{\rho_\infty} dy$
μ = dynamic viscosity
ν = kinematic viscosity
ρ = density
χ = hypersonic interaction parameter, $M_\infty^3/(Re_{x_\infty}/C)^{1/2}$
ψ = stream function
τ = $U_\infty t/x$

Subscripts

∞ = freestream value
w = quantity at the plate surface
1 = initial steady state
2 = final steady state

Superscripts

$'$ = differentiation with respect to η

A FIRST order perturbation solution for the temporal weak-interaction induced pressure was obtained in Refs. 1 and 2 for the case of a flat plate moving at hypersonic speed and subjected to an impulsive velocity increment of 1%. Whereas these solutions seem adequate for the calculation of the transient contribution to the induced pressure, this does not appear to be true for the estimation of the time-dependent component of the wall shear. The basic linearizing assumption of $\Delta f \ll f_2$, contained in Ref. 2, breaks down near $\tau = 0$ even when the fractional change in the plate velocity is small. The purpose of this Note is to report on a numerical solution to this problem without the use of a linearization procedure so that problems involving the accurate prediction of wall shear for plate velocity changes of 1% or larger may be treated.

The time-dependent boundary-layer equations, for zero pressure gradient and $Pr = 1$, in the transformed η, ξ plane are

$$2(1-\xi)^2 \frac{\partial f}{\partial \xi} - 2\xi(1-\xi)\left(f' \frac{\partial f'}{\partial \xi} - \frac{\partial f}{\partial \xi} f''\right) - ff'' - f''' = 0 \quad (1)$$

$$2(1-\xi)^2 \frac{\partial S}{\partial \xi}\left[1 - \frac{\xi f'}{(1-\xi)}\right] - S'' - S'\left[f - 2\xi(1-\xi)\frac{\partial f}{\partial \xi}\right] = 0 \quad (2)$$

(The coordinate system chosen is fixed with reference to the plate and its origin is at the leading edge.)

Equations (1) and (2) are similar to those given in Ref. 2 (before introduction of the assumption $\Delta f \ll f_2$), except for the definitions of the independent variable ξ and the dependent variable S. The solution of the momentum Eq. (1) is obtained by a numerical method.[3] Once the f' distribution is known, the S distribution may be obtained from

$$S(\eta,\xi) = f'(\eta,\xi) + S_w\{1 - f'(\eta,\xi)\} \quad (3)$$

which satisfies Eq. (2) and the relevant boundary conditions.

The numerical method, used here, is based on the Clutter-Smith technique[3] which solves the time-steady compressible laminar boundary-layer equations in two independent variables. This is an implicit finite-difference technique that is known to produce accurate results and has been well explored. In this method of solution the derivatives with respect to ξ (analogous to the spatial variable of Ref. 3 in the streamwise direction) are replaced by their finite-difference

Received April 12, 1971; revision received June 14, 1971. The authors would like to acknowledge the useful comments made by I. E. Beckwith during the preparation of the final manuscript.

Index category: Supersonic and Hypersonic Flow.

* Associate Professor, Mechanical Engineering.

† National Academy of Science Research Associate, Hypersonic Vehicles Division.

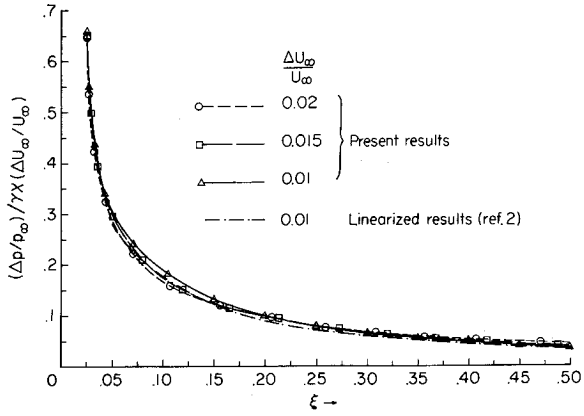

Fig. 1 Transient contribution to the induced pressure distribution for $S_w = 0$ and $M_\infty = 10$.

equivalents. When the solution has been obtained at all previous stations up to and including ξ_{m-1}, the problem is to find at the new station ξ_m the unknown derivative with respect to η (similar to the spatial variable of Ref. 3 normal to the surface) of the variable f' at the wall that satisfies the known outer boundary condition. The details of the method of integration at a particular ξ station are given in Ref. 3.

With the change in the plate velocity, the boundary layer existing on the plate surface undergoes reconfiguration and the following defect thicknesses are obtained:

$$\delta^*/[2\nu_\infty Cx/U_\infty]^{1/2} = \left\{1 + \left[\frac{(\gamma-1)}{2}\right] M_\infty^2\right\} I(\xi) \quad (4)$$

$$\delta_\rho/[2\nu_\infty Cx/U_\infty]^{1/2} = \left\{1 + \left[\frac{(\gamma-1)}{2}\right] M_\infty^2\right\} I(\xi) - J(\xi) \quad (5)$$

These expressions are valid for nonzero heat transfer at the plate surface. For the case of an adiabatic plate $S_w = 1$ must be used. From expressions (4) and (5) we notice that for the case of $M_\infty \rightarrow \infty$, δ^* approaches δ_ρ.

Following Ref. 1 we may finally write the expression for the induced pressure. In acoustic approximation this expression is

$$\frac{\Delta p_w}{p_\infty} = \frac{p_w - p_\infty}{p_\infty} = \frac{(2)^{1/2}}{M_\infty^2}\gamma\chi\left(1 + \frac{\gamma-1}{2}M_\infty^2\right) \times \left[\frac{I}{2} + (1-\xi)(1-2\xi)\frac{\partial I}{\partial \xi} - \frac{(1-\xi)^2}{\{1 + [(\gamma-1)/2]M_\infty^2\}}\frac{\partial J}{\partial \xi}\right] \quad (6)$$

If we choose the final steady state as the reference, the following expression is obtained:

$$\frac{(\Delta p/p_\infty)}{\gamma\chi} = \frac{(2)^{1/2}}{M_\infty^2}\left(1 + \frac{\gamma-1}{2}M_\infty^2\right)\cdot\left[\frac{(I_2 - I)}{2} - (1-\xi)(1-2\xi)\frac{\partial I}{\partial \xi} + \frac{(1-\xi)^2}{\{1 + [(\gamma-1)/2]M_\infty^2\}}\frac{\partial J}{\partial \xi}\right] \quad (7)$$

Expression (7) has been evaluated utilizing the $f'(\eta,\xi)$ distribution obtained from the numerical method mentioned previously. The fractional changes in the plate velocity considered are $\Delta U/U_\infty = 0.01$, 0.015, and 0.02. Figure 1 shows the plot of these numerical results for $M_\infty = 10$, $Pr = 1$, and $S_w = 0$. This figure also indicates that the transient contribution to the induced pressure decreases rapidly and monotonically with the increase in time for a given x. For the limiting case of $M_\infty \rightarrow \infty$, expression (7) reduces to

$$\frac{(\Delta p/p_\infty)}{\gamma\chi} = \left(\frac{\gamma-1}{(2)^{1/2}}\right)\left\{\frac{(I_2 - I)}{2} + (1-\xi)(1-2\xi)\frac{\partial I}{\partial \xi}\right\} \quad (8)$$

where

$$I(\xi) = \int_0^\infty (S_w + f')(1 - f')d\eta$$

and

$$I_2 = \int_0^\infty (S_w + f_2')(1 - f_2')d\eta$$

Numerical computations made by using expression (7) for $M_\infty = 10$ were found to be only very slightly different from those made by using expression (8).

In Fig. 2 is shown the distribution of the transient contribution to the shear function, $\Delta f''_w = f''_w$ (or $f''(0,\xi)$) $- f''_{w,2}$ (or $f''(0)$), where f''_w is related to the local skin-friction coefficient by the expression

$$C_f[Re_w/2]^{1/2} = f''(0,\xi) \quad (9)$$

where Re_w $(= U_\infty x/\nu_w)$ is the Reynolds number based on fluid properties evaluated at the wall temperature.

The curves of Fig. 2, like the induced pressure curves of Fig. 1, approach the steady-state value in a very rapid and monotonic way.

Results of Refs. 1 and 2 are also shown in Figs. 1 and 2. These figures show that the linearized procedure underpredicts the transient contribution to the shear stress by about 50% for smaller values of ξ's. However, the prediction of the temporal induced pressure by linearized procedure is smaller only by about 8% for $\xi \simeq 0.05$. It is also seen that the normalization of the results by the factor $(\Delta U_\infty/U_\infty)$ collapses the curves of Fig. 2 for different plate-velocity changes, on just one curve. The curves of Fig. 1 also exhibit a similar behavior within about 15%.

It should be noted that results are shown only for the region downstream of the contact line, $\xi = 0.5$. The results beyond this line are not obtainable due to the singular behavior of the differential equations at $\xi = 0.5$. Some idea of this singular nature may be obtained by examining the leading terms of the momentum Eq. (1)

$$\frac{\partial^2(f')}{\partial\eta^2} = 2(1-\xi)^2\left\{1 - \frac{\xi}{(1-\xi)}f'\right\}\frac{\partial(f')}{\partial\xi} + \cdots$$

The term in the curly bracket vanishes at $\xi = 1/(1 + f')$. Therefore, the discontinuity in the solutions should first appear at $f' = 1$ i.e. at the edge of the boundary layer with the corresponding value of ξ as 0.5.

In the region $0.5 \leq \xi \leq 1$, the problem should be formulated in terms of the Crocco variables and treated as a singular parabolic problem.[4] The present solutions may then be used to provide one set of boundary conditions at $\xi = 0.5$.

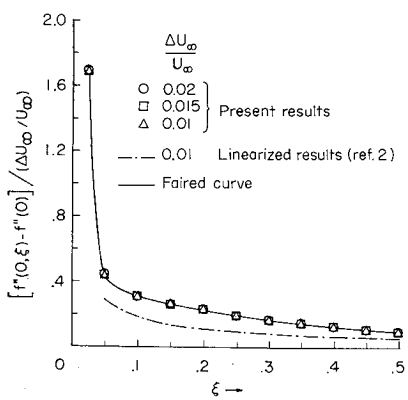

Fig. 2 Distribution of the transient contribution to the shear function.

The Blasius solution provides another boundary condition at $\xi = 1$.

References

[1] Reshotko, E. and Rodkiewicz, C. M., "Pressure Induced by Weak Interaction with Unsteady Hypersonic Boundary Layers," *AIAA Journal*, Vol. 7, No. 8, Aug. 1969, pp. 1609–1610.

[2] Rodkiewicz, C. M. and Reshotko, E., "Time-Dependent Hypersonic Viscous Interactions," Scientific Rept. 67-2451, Case Inst. of Technology FTAS/TR-67-28, Nov. 1967, Air Force Office of Scientific Research, Cleveland, Ohio.

[3] Clutter, W. D. and Smith, A. M. O., "Solutions of the General Boundary-Layer Equations for Compressible Laminar Flow Including Transverse Curvature," Rept. No. LB 31088, Revised Oct. 1964, Douglas Aircraft Co.; also *AIAA Journal*, Vol. 3, No. 4, April 1965, pp. 639–647.

[4] Ban, S. D. and Kuerti, G., "The Interaction Region in the Boundary Layer of a Shock Tube," *Journal of Fluid Mechanics*, Vol. 38, 1969, Pt. 1, pp. 109–125.

Ablation Surface Cross-Hatching on Cones in Hypersonic Flow

E. P. Williams* and G. R. Inger†
McDonnell Douglas Astronautics Company, Huntington Beach, Calif.

Introduction

The investigation reported herein was directed toward understanding and suppressing crosshatched patterns on ablating surfaces. A number of prior programs have been reported in Refs. 1–5. The objective of this particular study was to perform wind-tunnel experiments to assist in determining the source and mechanism of crosshatched patterns on ablating surfaces. Specifically, tests were made to satisfy the following objectives: 1) provide crosshatched patterns at higher edge Mach numbers and smaller cone angles than heretofore realized in ground-based tests and 2) determine the effect of nose bluntness on cross-hatching. Additional objectives beyond the scope of this Note will be found in the final contract report.[6] This work extends an earlier in-house effort (Ref. 5) to a more realistic simulation of the re-entry vehicle flight regime and geometry. The previous tests were all conducted at Mach 6 on sharp-nosed models, mostly camphor and Korotherm. As reported in Ref. 5, cross-hatching was obtained at lower surface pressures than anticipated. This made feasible the present tests at smaller cone angles and higher Mach numbers, and resulted in cross-hatching at an edge Mach number of 6.2, an appreciable increase over previous wind-tunnel data.

Description of Wind-Tunnel Ablation Tests

The tests were conducted in the Douglas Aerophysics Lab. 2-ft hypersonic wind tunnel at Mach numbers of 6, 8, and 10, on 6°, 10°, and 15° conical models. Schlieren, 35-mm still, and motion pictures were taken during each test. Models

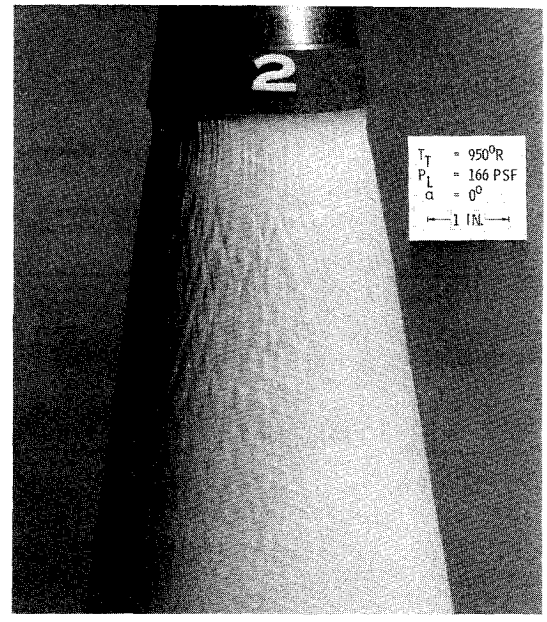

Fig. 1 10° camphor cone after 43 sec at $M_\infty = 6$.

were weighed and measured before and after each run to determine the amount of material lost resulting from ablation. Rubber molds and epoxy casts were made of the post-test models for a more permanent record of the ablated surface patterns.

Camphor and special Korotherm were chosen as the ablative materials, based upon the various materials tried in previous tests. Camphor worked well, even at the severe environment of Mach 10. For details on special fabricating techniques, etc., see Refs. 5 and 6. Clear camphor over black Noryl‡ cores gave good visual ablation surface pattern detail during testing, but only for a small area where the lighting was perfect. Consequently, ¼% of titanium dioxide was added to the powdered camphor before isostatic pressing to give a white or translucent ablation surface.

Korotherm was used primarily because of its previous performance at Mach 6. In its subliming mode it produced a wind-tunnel crosshatched pattern more similar to that of phenolic, fused-silica-fiber in flight than did camphor (Fig. 13 of Ref. 5). Unfortunately, no cross-hatching was obtained on Korotherm during the present tests, except for occasional local areas that ablated as a liquid. The cross-hatched pattern in these areas was wiped out by surface tension and solidification of the liquid layer at the end of the

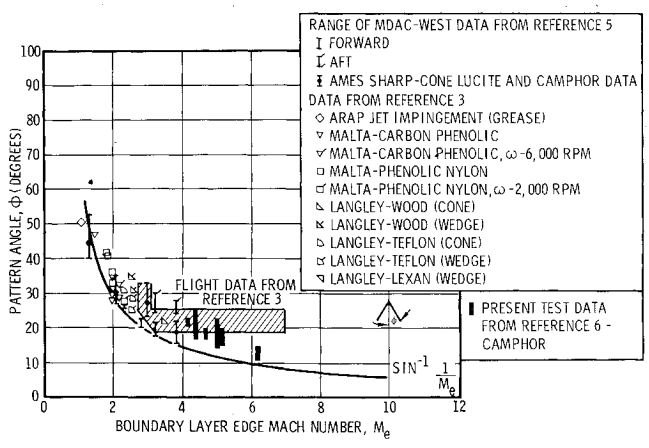

Fig. 2 Surface pattern angle as a function of local Mach number.

Received April 14, 1971. This work was sponsored by the Air Force Space and Missile Systems Organization under the Advanced Ballistic Re-Entry Systems Program Contract F04701-68-C-0288, Change Order P003.

Index categories: Rocket Vehicle Aerodynamics; Entry Vehicles and Landers; Material Ablation.

* Senior Staff Engineer, Special Aerodynamic Problems. Associate Fellow AIAA.

† Senior Staff Engineer, Fluid Physics. Now Professor of Aerospace Engineering, Virginia Polytechnic Institute and State University. Associate Fellow AIAA.

‡ Modified phenylene oxide thermoplastic resin.